LES OF LANGMUIR TURBULENCE IN STABLY STRATIFIED FLOW

Guillaume Martinat
Coastal Physical Oceanography
Old Dominion University
Norfolk VA
martinat@ccpo.odu.edu

Andres E. Tejada-Martínez
Civil & Environmental Engineering
University of South Florida
Tampa, FL.
aetejada@usf.edu

Chester E. Grosch
Coastal Physical Oceanography
Old Dominion University
Norfolk VA
enright@ccpo.odu.edu

ABSTRACT

Turbulent shear flows on shallow continental shelves (here shallow means that the interaction with the solid, no-slip bottom is important) are of great importance because of their role in vertical mixing as well as on the transport of sediment and bioactive material. The presence of a wave-field in these areas can lead to the appearance of Langmuir circulation (LC) which is known to strongly affect the dynamics of a turbulent flow. We investigate with large eddy simulation the influence of a stable stratification on Langmuir Circulation. Results show that LC intensity is reduced and then suppressed by an increasing statification.

INTRODUCTION

The interaction between surface gravity waves and a wind driven shear current can lead to the generation of longitudinal counter-rotating pairs of vortical structures. This phenomena is known as Langmuir circulation and was first identified by Irving Langmuir (1938). Langmuir circulation (LC) can be observed in any body of water with winds above $3ms^{-1}$ (Thorpe, 2004) and are characterized by the accumulation of foam and floating materials (windrows) at the surface convergence on top of the downwelling areas of the flow.

Using the CL model (Craik and Leibovitch, 1976), LES by Tejada-Martinèz and Grosch (2007), Martinat et al (2011) and Tejada-Martinèz et al (2012) amongst other have shown in various cases that the occurance of LC strongly affects the dynamic of the flow in the bottom boundary layer as well as the turbulence kinetic energy budgets, disrupting, for example, the log-law near the bottom.

The purpose of this study was to quantify via Large Eddy Simulation the effect of stable stratification on the dynamics of LC. Among the questions addressed are: does LC mix the water column and thus destroy the statification or does strong stratification substantially modify or eliminate LC?

GOVERNING EQUATIONS

Constant density flow is assumed because we assume that turbulent mixing is strong enough to remove stratification. The equations are solved in non-dimensional form. Let $(\ )^*$ denote a dimensional quantity and $(\ )$ a non-dimensional quantity. The velocity scale is $u^*_{\tau_T} \equiv \sqrt{\tau^*_T/\rho^*}$ with τ^*_T the total stress on the bottom, the length scale $\delta^* = H^*/2$, with H^* the water depth. The non-dimensional vertical coordinate is $-1 \leq x_3 \leq +1$ with this scaling. The velocity scale used in the non-dimensionalization is $u^*_{\tau_T}$ so the Reynolds number in the non-dimensional equations is Re_{τ_T}.

The spatially filtered (denoted by the overline) Craik-Leibovich equations, including the buoyancy term with the Boussinesq approximation, and the density conservation equation are

$$\frac{\partial \bar{u}_i}{\partial x_i} = 0, \tag{1}$$

$$\frac{\partial \bar{u}_i}{\partial t} + \bar{u}_j \frac{\partial \bar{u}_i}{\partial x_j} = -\frac{\partial \bar{\Pi}}{\partial x_i} - Ri_\tau \bar{\rho}\, \delta_{i3} + \frac{1}{Re_\tau}\frac{\partial^2 \bar{u}_i}{\partial x_j^2} + \frac{\partial \tau_{ij}}{\partial x_j} + \frac{1}{La_t^2}\varepsilon_{ijk} V_j^s \bar{\omega}_k, \tag{2}$$

$$\frac{\partial \bar{\rho}}{\partial t} + \left(\bar{u}_j + \frac{1}{La_t^2}V_j^s\right)\frac{\partial \bar{\rho}}{\partial x_j} = \frac{1}{Pr\, Re_\tau}\frac{\partial^2 \bar{\rho}}{\partial {x_j}^2} + \frac{\partial \lambda_j}{\partial x_j}, \tag{3}$$

The non-dimensional pressure is $\bar{\Pi} = \bar{p} + \frac{1}{2}\bar{P} = \bar{p} + \frac{1}{2}\left[\frac{1}{La_t^4}V_i^s V_i^s + \frac{2}{La_t^2}\bar{u}_i V_i^s\right]$, where $\bar{p}$ is the non-dimensional dynamic pressure and $\bar{P}$ is the Bernoulli head arising from the C-L averaging process of the non-linear terms. The constant reference density, ρ^*_o, and the corresponding hydrostatic pressure gradient term have been subtracted from the momentum equation so that $\bar{p}$ and $\overline{\rho}$ in the momentum equation are the dynamical quantities.

In these equations τ_{ij} is the subgrid-scale stress, $La_t = \sqrt{u_\tau^*/V_o^{s*}}$ the turbulent Langmuir number, Re_τ the Reynolds number based on u_τ^* and δ^*, λ_j the subgrid-scale buoyancy flux term analogous to τ_{ij} and the Prandtl number, $Pr = \nu^*/\kappa^*$. The non-dimensionalized C-L vortex force is the fifth term on the right hand side of equation (2).

The second term on the right hand side of equation (2) is the buoyancy term where the Richardson number is $Ri_\tau \equiv \left(\frac{g^*\delta^*}{(u_\tau^*)^2}\right)\left(\frac{\Delta\rho^*}{\rho_0^*}\right) = \frac{(N^*)^2}{(S^*)^2}$, with $(N^*)^2 = (g^*/\rho_0^*)(\Delta\rho^*/\delta^*)$ the square of the buoyancy frequency and $S^* = u_\tau^*/\delta^*$ the shear. The Richardson number is the measure of the strength of the stratification. Increasing $\Delta\rho^*$, and thus the magnitude of the stratification, increases Ri_τ. Because the dimensional fluctuating density is scaled by $\Delta\rho^*$ the non-dimensional density $\overline{\rho}$ lies in the range $(0,1)$. As $\Delta\rho^*$ and $Ri_\tau \to 0$, $\overline{\rho}$ tends to a passive scalar. For small but non-zero Ri_τ, $\overline{\rho}$ is a dynamic quantity having only in a minor effect on the momentum balance. A large Ri_τ, and hence a strong stratification, is expected to result in a major change in the dynamics of the flow.

Boundary and Forcing Conditions

This LES employs a free surface boundary condition for the vertical component of the velocity of the first type; we specify $\bar{u}_3(x_1,x_2,+1) = 0$. The other boundary conditions for the velocity on the free surface are $\partial\bar{u}_1/\partial x_3 = Re_\tau$, which incorporates the prescribed wind stress forcing, and $\partial\bar{u}_2/\partial x_3 = 0$ on $x_3 = +1$. On the bottom, $x_3 = -1$, $\bar{u}_i = 0$. The boundary conditions for the perturbation density, $\overline{\rho}$, are $\overline{\rho} = 0$ at $x_3 = +1$ and $\overline{\rho} = 1$ at $x_3 = -1$ and so the density field evolves along with the velocity but, overall, remains stably stratified. At a later date we intend to carry out LES of a somewhat more realistic model of a stably stratified flow; one in which the stable stratification is caused by imposing a flux of heat into the free surface.

Parameters

The LES were carried out for $Re_\tau = 395$ with $La_t = 0.7$, a wavelength of $6H^*$, $Ri_\tau = 0, 8, 16, 32, 64, 128, 256$ and 512. For most of the LES $Pr = 1.0$ but in order to examine the effect of changing Pr, LES were also carried out with $Pr = 3.0, 5.0$ and 7.5 for $Ri_\tau = 32$ and with the same values of Re_τ, La_t and the wavelength. Water at a temperature of 18.5C has $Pr = 7.5$. The Pr values of 3.0 and 5.0 are intermediate and were chosen to show the changes as Pr was increased from 1.0.

The presence of stratification required the addition of the buoyancy term, $-Ri_\tau\overline{\rho}\,\delta_{i3}$, to the momentum equation.

Numerical Method

The numerical method used to solve the governing equations combines 2^{nd} order fractional time stepping with a hybrid spatial discretization. The spatial discretization is spectral in the x_1 and x_2 directions with 5^{th} and 6^{th} order compact differencing and grid stretching in the x_3 direction. The SGS stress is represented by the the dynamic Smagorinsky closure (Smagorinsky, 1963; Lilly, 1992). The details of the method used to solve the governing equations, including the temporal and spatial discretization, the grid stretching, the finite-difference stencils, the SGS stress and the parallel implementation, is described in detail in Appendices E and F of TMG07.

RESULTS

Global properties

The bulk Reynolds and Richardson numbers for the various values of Ri_τ are listed in Table 1. Increasing Ri_τ results in an increase in both Re_b and Ri_b because of the increase in the mean speed, U_b, particularly in the upper half of the water column, see figure (1). As Ri_τ increases Re_b increases by somewhat more than a factor of three between $Ri_\tau = 0$ and 512. The near bottom boundary layer is little modified by the increase in Ri_τ because the surface stress is held fixed as Ri_τ is varied and consequently the stress on the bottom must remain constant in order to balance the surface stress. Therefore, the mean profile in the viscous sublayer must also be unchanged. The near surface boundary layer is also similar in that the slope of the mean profile is set by the imposed stress for all values of Ri_τ. However in the remainder of the water column, $\langle\bar{u}_1\rangle$ approaches a linear profile as Ri_τ increases. If the flow were laminar the flow would be, in the absence of the C-L force, a form of stratified Couette flow. The unstratified Couette flow is stable to infinitesimal disturbances for all wavenumbers and Reynolds numbers (Drazin and Reid [1981]). For the inviscid, stratified case a necessary condition for instability is the $Ri_b < 1/4$ (Chandrasekhar, [1961]). For the viscous stratified Couette flow, the stability/instability depends on the form of the density profile and no general condition for instability seems to be known. However, the small values of Ri_b and the relatively large values of Re_b for these LES suggest that the flow is unstable, thus turbulent. Our results are in accord with this supposition.

Table 1 also lists the total energy, E, the mean kinetic energy, MKE, the turbulent kinetic energy TKE and the potential energy PE. Also listed is the fraction, in %, of each component of the total energy as Ri_τ varies. Even though the forcing, the surface stress, is held constant E increases markedly with increasing Ri_τ because of the increase in the mean velocity. with the increase in Ri_τ. The other effect of increasing Ri_τ is to substantially modify the balance of the components of E. The potential energy increases and the mean kinetic energy decreases, as a fraction of the total energy, as Ri_τ increases. The turbulent kinetic energy also decreases as a fraction of total energy from almost 6% at $Ri_\tau = 0$ to less that 1% of the total at $Ri_\tau = 256$ and only 0.5% at $Ri_\tau = 512$; a decrease of more than an order of magnitude as compared to $Ri_\tau = 0$. The increased stratification is acting so as to ”damp” the turbulent fluctuations and, hence, the TKE.

Mean velocity profiles

Figure (1) shows the mean velocity profiles (left panel) and profiles of the mean density (right panel) for the various values of Ri_τ. As Ri_τ is increased the mean velocity at the surface increases. The magnitude of the increase in the surface speed between $Ri_\tau = 0$ and $Ri_\tau = 512$ is approximately a factor of three. Noting that, if the flow were laminar the mean velocity and density profiles would be linear, the increase of $\langle\bar{u}_1\rangle$ as Ri_τ increases suggests a tendency for the flow to evolve towards a laminar-like state. The surface stress driving the flow is independent of Ri_τ so the bottom stress that balances the surface stress must also be independent of Ri_τ, as is evident in all of these profiles. The in-

Re_τ	Ri_τ	Re_b	Ri_b	E	MKE (%)	TKE (%)	PE (%)
395	0	7292	0.0	180.88	94.2	5.8	0.0
	8	7692	0.0211	202.55	93.6	4.8	1.6
	16	7930	0.0397	216.72	93.0	4.1	2.9
	32	8583	0.0678	256.64	92.0	3.0	5.0
	64	10481	0.0909	387.06	90.9	2.0	7.0
	128	12937	0.1193	596.85	89.9	1.4	8.8
	256	16651	0.1441	1003.76	88.5	0.8	10.7
	512	21545	0.1721	1717.28	86.6	0.5	12.9

Table 1. Variation with the stress Richardson number, Ri_τ, of the bulk Reynolds number, Re_b, and bulk Richardson number, Ri_b, the total energy, E and, in % of the total, the mean kinetic energy, MKE, turbulent kinetic energy, TKE, and potential energy, PE. In all cases $Pr = 1.0$.

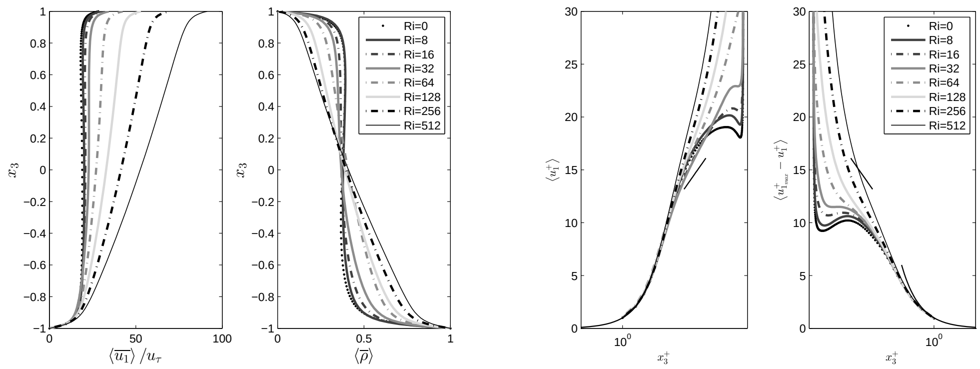

Figure 1. *Mean velocity, $\langle \overline{u}_1 \rangle$, and density, $\langle \overline{\rho} \rangle$, profiles with various values of Ri_τ (left). Mean velocity and density profiles from the LES with the various values of Ri_τ in terms of viscous or 'wall' variables. In the left panel x_3^+ is measured upward from the bottom so that $x_1^3 = 0.1$ is close to the bottom. In contrast, in the right panel x_3^+ is measured downward from the surface so that $x_1^3 = 0.1$ is close to the surface.(right)*

crease in the mean velocity away from the solid boundary as Ri_τ is increased is in general agreement with the results of Armenio & Sarkar [2002]; see their figure (5) and note that they are simulating a flow in a channel with solid no-slip upper and lower boundaries resulting in the symmetry of the profiles. This is in contrast to this simulation with only a solid no-slip bottom.

When $Ri_\tau = 0$ the density is a passive scalar but for $Ri_\tau > 0$ the density is a dynamic variable that is coupled to the velocity. For all Ri_τ the structure of the density profiles (right hand panel of figure (1)) is similar. For $Ri_\tau = 0$ and 8 most of the water column is well mixed with the density distribution almost constant in $-0.8 \leq x_3 \leq 0.8$. There are also near surface and near bottom layers with large gradients resulting from the boundary conditions that $\langle \overline{\rho} \rangle = 0$ at the surface and 1.0 at the bottom. As Ri_τ increase the vertical mixing decreases because of the increased strength of the stratification resulting in an increase in the density gradient in the interior and a thickening of the near surface and bottom layers. For $Ri_\tau \geq 64$ the gradient is nearly constant in most of the water column. The increase in the steepness of the density gradient as Ri_τ increases is due to the increasing stabilization of the flow with increasing strength of the stratification. Again, these results are in general agreement with the density profiles of Armenio & Sarkar [2002] as can be seen from their figure (6).

Autocorrelation functions

The same pattern of one, then two, then four LC cells in the upper part of the water column as Ri_τ is increased accompanied by the disappearance of LC cells in the lower part of the water column is seen in the autocorrelation functions. The two-point, one-time, streamwise correlation function is defined as

$$R^x_{\alpha\beta}(\Delta x_1, x_3) = \frac{\left\langle \vec{u}'_\alpha(t, x_1, x_2, x_3) \vec{u}'_\beta(t, x_1 + \Delta x_1, x_2, x_3) \right\rangle_{x_2,t}}{\left\langle \vec{u}'_\alpha \vec{u}'_\beta \right\rangle}. \quad (4)$$

Similarly, the spanwise correlation function is

$$R^y_{\alpha\beta}(\Delta x_2, x_3) = \frac{\left\langle \vec{u}'_\alpha(t, x_1, x_2, x_3) \vec{u}'_\beta(t, x_1, x_2 + \Delta x_2, x_3) \right\rangle_{x_1,t}}{\left\langle \vec{u}'_\alpha \vec{u}'_\beta \right\rangle}, \quad (5)$$

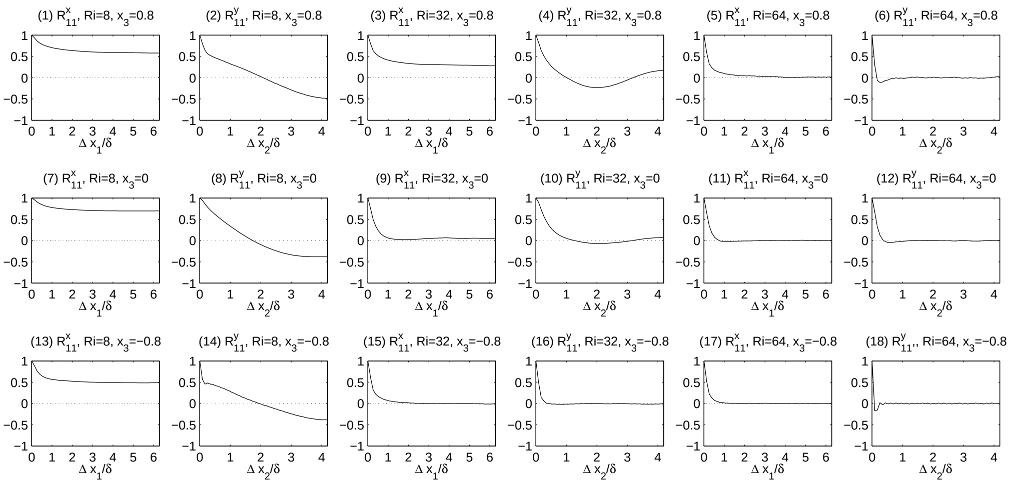

Figure 2. *streamwise correlation functions, R^x_{11}, the cross-stream correlation functions, R^y_{11}, for $Ri = 8, 32, 64$. The upper line (panels 1-6) show these correlations functions in the upper part of the water column, $x_3 = 0.8$. The middle line (panels 7-12) show these correlations functions at mid-depth, $x_3 = 0$. And the lower line (panels 13-18) show these correlations functions in the lower part of the water column, $x_3 = -0.8$.*

where $\langle\cdot\rangle_{x_i,t}$ denotes averaging in time and over the x_i-direction. Autocorrelations are obtained by setting $\beta = \alpha$ in (4) and (5) and ignoring the usual convention of summing over repeated indices. The streamwise correlation functions, R^x_{11} and the cross-stream correlation functions, R^y_{11} at three depths, near surface ($x_3/H = 0.9$), mid-depth ($x_3/H = 0.5$) and near bottom ($x_3/H = 0.1$) are shown in figures (2) for, respectively, $Ri_\tau = 8, 32$, and 64.

With $Ri_\tau = 8$, figure (2), the correlation functions are very nearly identical to those reported by TMG07 of an LES of LC in unstratified flow (see figures (5), (6) and (7) of TMG07). R^x_{11} is substantially greater than zero and constant for $\Delta x_1/\delta > 1$ at all depths. The structure of R^y_{11} and R^y_{22} show, by the zero-crossings at $\Delta x_2/\delta \approx 2$, the presence of a single LC at all depths. One can conclude that the weak stratification that exists for $Ri_\tau = 8$ has almost no effect on LC.

In contrast, for $Ri_\tau = 32$ there is a major change in the correlation functions seen in figure (2). With $Ri_\tau = 32, R^x_{11}$ is roughly constant in $\Delta x_1/\delta > 1.5$ at all depths but the magnitudes of the R^x_{11} are somewhat smaller for this case as compared to that of $Ri_\tau = 8$. The increased stratification effectively destroys the correlation in the streamwise, x_1, direction. In contrast, in the upper two regions the two zero crossings of R^y_{11} shows the presence of two LC cells. Near the bottom there is no evidence of any LC cells in the R^y_{11}. In short, the correlation functions are clear evidence of two cell LC near the surface and at mid-depth but the complete absence of LC cells near the bottom. Finally, with $Ri_\tau = 64$, almost all of the correlation functions decay rapidly with increasing $\Delta x_1/\delta$ or $\Delta x_2/\delta$; the $R^x_{\alpha,\alpha}$ are ≈ 0 for $\Delta x_1/\delta > 2$. The only exception is R^x_{11} at $x_3/H = 0.9$. R^x_{11} decreases with increasing $\Delta x_1/\delta$ but only to about 0.1 at the end of the domain. The further increase in the strength of the stratification with $Ri_\tau = 64$ destroys the correlation. In the near surface and mid-depth regions R^y_{11} is very small but has four small oscillations and associated zero crossings, indicating the presence of four weakly correlated LC cells in the upper 1/4 to 1/2 of the water column. Taken together, the structure of the correlation functions suggest the existence of four weak LC cells that are mildly correlated in the streamwise direction.

In summary, the correlation functions provide clear evidence of the increase in the number of LC cells as Ri_τ is increased.

Map of the invariants of the Reynolds stresses

The resolved Reynolds anisotropy tensor is (Lumley, [1978]; Pope, [2000])

$$b_{ij} = \frac{\left\langle \overline{u}'_i \overline{u}'_j \right\rangle}{2k} - \frac{1}{3}\delta_{ij}, \qquad (6)$$

where k is the resolved turbulent kinetic energy. The first invariant $\mathrm{I} = \mathrm{trace}\{b_{ij}\} = 0$. The second and third invariants are $\mathrm{II} = b_{ij}b_{ji}$ and $\mathrm{III} = b_{ij}b_{jk}b_{ki}$. The quantity $\mathrm{II}^{1/2}$ is a measure of the magnitude of the anisotropy, while the location of the coordinate $(\mathrm{II}^{1/2}, \mathrm{III}^{1/3})$ serves as a measure of the shape of the anisotropy and thus the state of the resolved turbulence. A clear and concise description of the Lumley triangle and the corresponding states of the Reynolds anisotropy tensor was presented by Simonsen & Krogstad, [2005].

The trajectory in figure (3) for $Ri_\tau = 0$ is identical to that of figure (13a) of TMG07. It is reproduced here for comparison with the trajectories having $Ri_\tau \neq 0$. Very close to the bottom wall the fluctuating motion is two component (near the right hand side of the top bounding curve of the Lumley triangle) because $\langle \overline{u}'_3 \overline{u}'_3 \rangle$ is much smaller than the other two normal Reynolds stress components. As distance from the wall increases the trajectory moves towards the one component state as $\langle \overline{u}'_1 \overline{u}'_1 \rangle$ increases relative to $\langle \overline{u}'_2 \overline{u}'_2 \rangle$. However, just above the viscous sub-layer, $x_3^+ \approx 7$, the trajectory reverses direction, moving somewhat into the interior near the left hand side and towards the state of two component isotropic turbulence. The reason for this behavior is that $\langle \overline{u}'_1 \overline{u}'_1 \rangle$ and $\langle \overline{u}'_2 \overline{u}'_2 \rangle$ are much greater

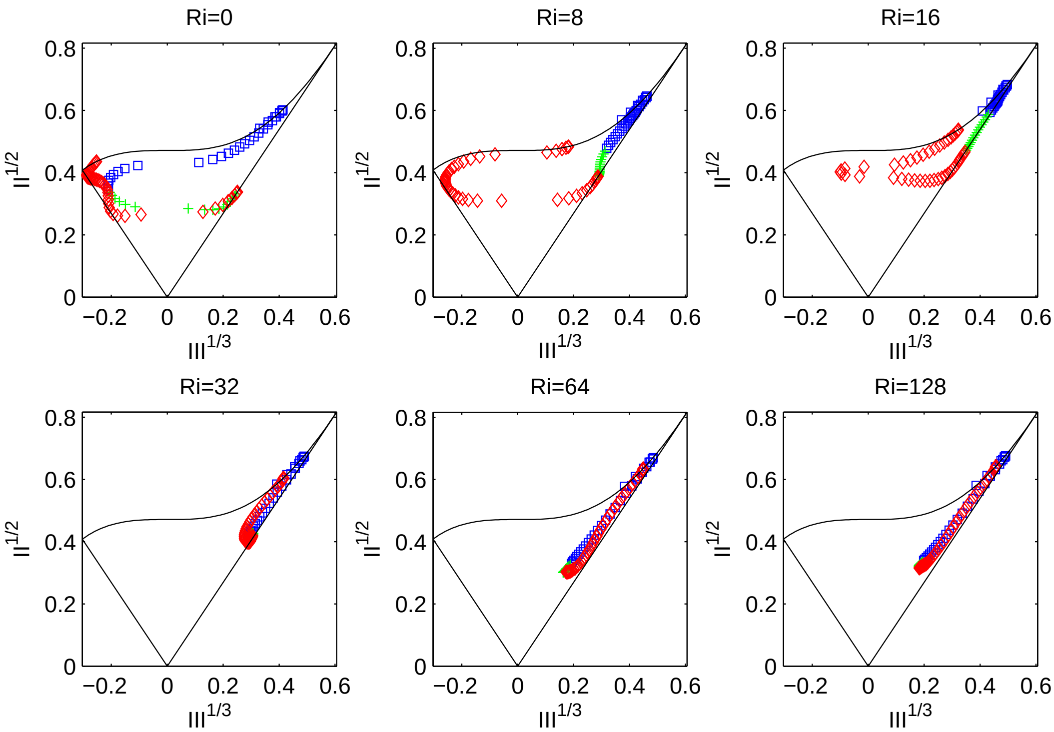

Figure 3. *Trajectories of the invariants of the resolved Reynolds stress anisotropy tensor for* $Ri_\tau = 0, 8, 16, 32$ *and* 64. *The symbols indicate position within the water column:* $\square$, $x_3/H \in (0,1/3]$; $+$, $x_3/H \in (1/3,2/3]$; $\diamond$, $x_3/H \in (2/3,1]$. *In all cases* $Re_\tau = 395$.

than $\langle \bar{u}_3'\bar{u}_3' \rangle$ throughout most of the bottom third portion of the water column. This is no longer true in the region $0.35 < x_3 < 0.45$ as the ordering $\langle \bar{u}_1'\bar{u}_1' \rangle > \langle \bar{u}_3'\bar{u}_3' \rangle \approx \langle \bar{u}_2'\bar{u}_2' \rangle$ holds and the turbulence shifts back to an axisymmetric cigar-shape state. In the upper-half of the water column, as distance to the top surface decreases, the turbulence moves back to the pancake-shape state. At the surface, the turbulence assumes an approximately two component isotropic state (the upper left hand side vertex of the triangle) because $\langle \bar{u}_1'\bar{u}_1' \rangle \approx \langle \bar{u}_2'\bar{u}_2' \rangle$ and $\langle \bar{u}_3'\bar{u}_3' \rangle = 0$.
As Ri_τ is increased from zero, the trajectory is substantially changed. A modest increase in stratification, to $Ri_\tau = 8$, modifies the structure of the turbulence in most of the water column. The trajectory very close to the bottom, $x_3^+ < 7$, is unchanged but above this region the trajectory shifts close to the right hand boundary; that with the cigar-shaped state. The state in the middle third of the water column is nearly identical to that in the region below. Only in the upper third of the water column is there evidence of a substantially three component structure. The trajectory moves into the interior of the triangle forming a C-shape. It terminates on the left hand boundary (the pancake-shaped state) midway between the two and one component states. The change in the trajectory shows that even modest stratification has an important effect on LC throughout the water column and especially in the lower two-thirds of it.
With $Ri_\tau = 16$ the C-shaped portion of the trajectory is much reduced in size as compared to $Ri_\tau = 8$. It entirely collapses with $Ri_\tau = 32$. Finally, the trajectories are essentially identical for the cases with $Ri_\tau = 32$ and 64. They both are virtually identical to, first, the trajectory of a wind stress driven flow without the CL force that is shown in figure (13b) of TMG07 and, second, to the trajectories for cases of combined wind stress without the CL force and pressure gradient driven flows, both with the wind stress and pressure gradient colinear and normal to each other, Martinat *et al.*, [2011].
Clearly the increase in stratification effectively suppresses LC as shown by the major distortion of the trajectory of the invariants with the increase in Ri_τ. If the flow is unstratified or only weakly stratified the trajectory of the invariants is a sensitive diagnostic for the presence or absence of LC. However, if the stratification is strong the trajectory of the invariants shows that the turbulence structure is not sensitive to the forces driving the flow.

DISCUSSION AND CONCLUSION

This LES of LC in a stably stratified shallow water flow was carried out with the Richardson number, Ri_τ, characterizing the strength of the stratification varied from 0, a homogeneous water column, to 512, a strongly stratified water column. It was found that weak stratification, $Ri_\tau \le 16$, caused minor variation in the mean profile and correspondingly small changes in the mean density profile. Overall, the increase in Ri_τ from 0 to 512 results in an increase in the magnitude of the surface speed by approximately a factor of three. The mean velocity profile is close to linear throughout most of the water column for the larger values of Ri_τ. Even though the surface stress is constant the total energy increases markedly with increasing Ri_τ because of the increase in the mean velocity in most of the water column. As Ri_τ increases there is a corresponding increase in the bulk Reynolds number and decrease in the bulk Richardson numbers. Another effect of increasing Ri_τ is to substantially modify the balance of the components of total energy. The potential energy increases and the mean kinetic energy, as a fraction of the total energy, decreases as Ri_τ increases. The potential energy increased from 0 at $Ri_\tau = 0$ to 12.9% of the total energy at $Ri_\tau = 512$. The turbulent kinetic energy decreases as a fraction of total energy from almost 6% at $Ri_\tau = 0$ to less than 0.5% of the total at $Ri_\tau = 512$. The increased stratification acts to "damp" the turbulent fluctuations and, hence, the TKE. The observed decrease in the TKE suggests that the bulk Richardson number is tending towards a stability boundary, perhaps $Ri_b = 0.25$, above which the flow will be laminar.

For $Ri_\tau = 0$ and 8 most of the water column is well mixed with the mean density distribution almost constant in $-0.8 \leq x_3 \leq 0.8$. There are also near surface and near bottom layers with large gradients resulting from the boundary conditions that $\langle \overline{\rho} \rangle = 0$ at the surface and 1.0 at the bottom. As Ri_τ increase the vertical mixing decreases because of the increased strength of the stratification resulting in an increase in the density gradient in the interior and a thickening of the near surface and bottom layers. For $Ri_\tau \geq 64$ the gradient is nearly constant in most of the water column. The increase in the steepness of the density gradient as Ri_τ increases is due to the increasing stabilization of the flow with increasing strength of the stratification. Again, these results are in general agreement with the density profiles of Armenio & Sarkar [2002] as can be seen from their figure (6).

The same changes in cell structure is also shown by the autocorrelation functions. The single cell structure for $Ri_\tau = 8$, the two cell structure when $Ri_\tau = 32$ and the very weak four cell structures for $Ri_\tau = 64$ are apparent. The 'quantization" of the number of cells, however is probably induced by the imposition of periodic boundary conditions in the cross-stream direction in the LES. In the ocean the width of the domain is not fixed so one would expect that increasing the stratification wouldn't have this 'quantized' effect. As stratification increased the effective depth of the surface LC layer would change continuously and the scale and number of the LC cells in that layer would adjust so as to have their width three to four times the effective depth. This process can not continue indefinitely because the decreasing vertical and horizontal size of the cells increase the velocity gradients thereby increasing the viscous dissipation. At some small size the dissipation of LC turbulent kinetic energy outweighs the production by the Craik-Leibovich vortex force and LC is turned off. It appears that the LC cells are greatly weakened for $Ri_\tau \geq O(64)$.

The trajectory with depth of the invariants of the Reynolds stress anisotropy tensor was found to be an extremely sensitive diagnostic of the change in the flow structure as Ri_τ was varied. The increase of Ri_τ from 0 to 8 caused a major change. The counter-clockwise, C-shaped trajectory beginning along the upper, two component boundary that is observed in the lower two-thirds of the water column with $Ri_\tau = 0$ vanishes when $Ri_\tau = 8$. In its place is a clockwise C-shaped trajectory in the upper third of the water column. As Ri_τ is increased this C-shaped trajectory shrinks and then collapses onto the two component side of the triangle with $III > 0$ when $Ri_\tau = 32$. The trajectory is indistinguishable from that of a pressure gradient driven flow or a surface stress driven flow without the C-L force. There is no additional change in the trajectory as Ri_τ is increased further. The behavior of the trajectory of the invariants can be interpreted as showing that the LC cells are so weakened by the stratification that they are unimportant to the dynamics for $Ri_\tau \geq 32$.

We conclude that increasing the strength of the stratification, *i.e.* Ri_τ, under constant wind stress forcing caused major changes in the mean velocity and density profile. The magnitude of the surface speed increased by approximately a factor of three as Ri_τ was increased from 0.0 to 512.0 and the mean velocity profile evolved to a nearly linear one throughout most of the water column. The structure of the mean density profiles is similar for all $Ri_\tau \neq 0$. As Ri_τ was increased the magnitude of the total energy increased markedly with the mean kinetic energy, as a fraction of the total energy, decreasing slightly; the TKE decreased as a fraction of total energy from almost 6% at $Ri_\tau = 0$ to 0.5% of the total at $Ri_\tau = 512$ and the potential energy increasing from 0% to 12.9% of the total energy at the largest value of Ri_τ. The increased stratification acts to "damp" the turbulent fluctuations and, hence, the TKE. As Ri_τ increases there is a corresponding increase in the bulk Reynolds and Richardson numbers. The LC is strongly modified by increasing the stratification. Depending on which diagnostic is used, it was found that LC was almost totally "shut down" for Ri_τ in the range 32 to 64.

Aknowledgement

The support of the National Science Foundation through grant OCE 0927724 is gratefully acknowledged.

REFERENCES

Armenio, V. and Sarkar, S. [2002] An investigation of stably stratified turbulent channel flow using large-eddy simulation. J. Fluid Mechanics **459**, 1-42.

Craik, A.D.D. & Leibovich, S. A rational model for Langmuir circulation. *J. Fluid Mech.* **73**, 401-426, 1976.

Langmuir, I. Surface motion induced by the wind. *Science* **87**, 119-123, 1938.

Lilly, D.K. A proposed modification of the Germano subgrid-scale closure. *Physics of Fluids* **3**, 2746-2757, 1992.

Lumley, J.L. Computational modeling of turbulent flows. In *Advan. App. Mech.*, **18**, 123-176, 1978.

Martinat, G. & Xu, Y. & Grosch, C.E. & Tejada-Martínez, A. E. LES of turbulence surface shear stress and pressure-gradient driven flow on shallow continental shelves. *Ocean Dynamics* **61**, 1369-1390, 2011

Pope, S.B. *Turbulent Flows.* Cambridge University Press, 2001.

Simonsen, A.J. and Krogstad, P.-Å. [2005] Turbulent stress invariant analysis: Clarification of existing terminology. Physics of Fluids **17**, 088103-1 - 088103-4.

Smagorinsky, J. General circulation experiments with the primitive equations. I. The basic experiment. *Mon. Wea. Rev.* **91**, 99-164, 1963.

Tejada-Martínez, A. E. & Grosch, C.E. Langmuir turbulence in shallow water. Part 2. Large-eddy simulation *J. Fluid Mech.* **576**, 63-108, 2007.

Tejada-Martínez, A. E. & Grosch, C.E. & Sinha, N & Akan, C. & Martinat. G. Disruption of bottom log-layer in LES of full-depth Langmuir circulation. *J. Fluid Mech.*, **699**, 79-93, 2012.

Thorpe, S. Langmuir circulation. *Annu. Rev. Fluid Mech.* **35**, 55-79, 2004.